Supporting Information

Gaseous infrared spectra of the simplest geminal diol $CH_2(OH)_2$ and the isotopic analogues in the hydration of formaldehyde

*Hung-Yang Jain, Chih-Tsun Yang and Li-Kang Chu**

Department of Chemistry, National Tsing Hua University, 101, Sec. 2, Kuang-Fu Rd., Hsinchu 30013, Taiwan.

Corresponding Author

*To whom correspondence should be addressed. Phone: 886-3-5715131 ext. 33396. Fax: 886-3-5711082. E-mail: lkchu@mx.nthu.edu.tw

Table of contents

Supplementary Tables

Supplementary Figures

Table S1. The partial pressures (Torr) of the samples for the infrared spectroscopic measurements.

	$CH_2(OH)_2$	$CD_2(OH)_2$	$CH_2(OD)_2$	$CD_2(OD)_2$
$P(H_2O)$	20.1	26.3		
$P(D_2O)$			12.2	19.3
$P(CH_2O)$	9.8		6.9	
$P(CD_2O)$		9.6		8.6
$P(N_2)$	11.0	69.0	8.9	69.0
Total pressure	40.9	104.9	28.0	96.9

Table S2. Optimized molecular structures of *trans*-$CH_2(OH)_2$ and *cis*-$CH_2(OH)_2$ determined with B3LYP/aug-cc-pVTZ in vacuum. The predictions at the level of CCSD(T) using the basis set aug-cc-pVTZ [1] are included for comparison. (bond length (*d*): angstrom; bond angle (∠): degree; dihedral angle (*ϕ*): degree).

Parameter	*trans*-$CH_2(OH)_2$			*cis*-$CH_2(OH)_2$		
	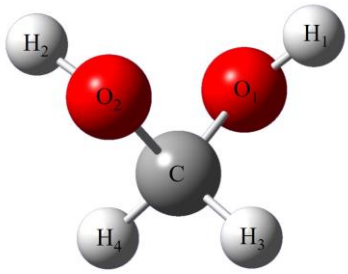			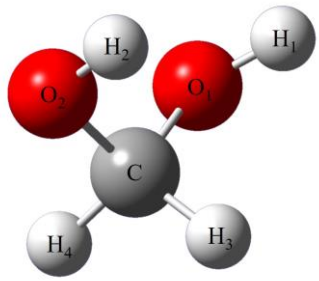		
	B3LYP	CCSD(T)*	Δ (%)	B3LYP	CCSD(T)*	Δ (%)
Point group	C_1	C_2		C_1	C_s	
$d(C–O_1)$	1.4082	1.4085	–0.021	1.4092	1.4092	0.000
$d(C–O_2)$	1.4081		–0.028	1.4091		–0.007
$d(O_1–H_1)$	0.9635	0.9639	–0.042	0.9620	0.9624	–0.042
$d(O_2–H_2)$	0.9636		–0.031	0.9620		–0.042
$d(C–H_3)$	1.0914	1.0922	–0.073	1.0954	1.0961	–0.064
$d(C–H_4)$	1.0914	1.0922	–0.073	1.0866	1.0876	–0.092
$\angle O_1CO_2$	112.9942	112.61	0.340	113.9044	113.61	0.258
$\angle H_1O_1C$	108.5327	107.42	1.025	109.9392	108.87	0.973
$\angle H_2O_2C$	108.5351		1.027	109.9427		0.976
$\angle H_3CO_2$	105.1985	105.29	–0.087	110.4953	110.47	0.023
$\angle H_3CO_1$	111.7888		5.813	110.4816		0.010
$\angle H_4CO_1$	105.2043	105.29	–0.081	105.8779	106.00	–0.115
$\angle H_4CO_2$	111.7861		5.811	105.8708		–0.122
$\phi H_1O_1CO_2$	62.7796	61.75	1.640	79.2727	78.63	0.811
$\phi H_2O_2CO_1$	62.7907	61.75	1.657	–79.0590	–78.63	0.543
$\phi H_3CO_2O_1$	122.2166	122.08	0.112	125.0489	124.79	0.207
$\phi H_4CO_1O_2$	122.2171	122.08	0.112	115.9168	116.0	–0.072

*: Ref. 1; Δ = 100 × [B3LYP – CCSD(T)] / B3LYP.

Table S3. Optimized molecular structures of *trans*-$CH_2(OH)_2$ determined with B3LYP/aug-cc-pVTZ in vacuum. The predictions at the level of MP2 using the basis set aug-cc-pVTZ [2] are included for comparison. (bond length (*d*): angstrom; bond angle (∠): degree).

Parameter	*trans*-$CH_2(OH)_2$ (C_1)		
	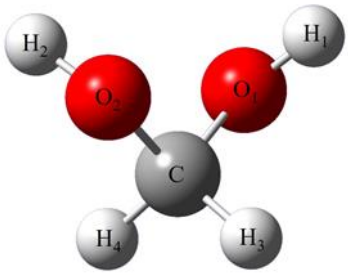		
	B3LYP	MP2*	diff. (%)
d(C–O_1)	1.4082	1.4066	0.114
d(C–O_2)	1.4081	1.4065	0.114
d(C–H_3)	1.0914	1.0890	0.220
d(C–H_4)	1.0914	1.0890	0.220
d(O_1–H_1)	0.9635	0.9639	–0.042
d(O_2–H_2)	0.9636	0.9639	–0.031
∠H_1O_1C	108.5327	107.3950	1.048
∠H_2O_2C	108.5351	107.3927	1.053
∠O_1CO_2	112.9942	112.7767	0.192
∠H_3CH_4	109.9782	110.2472	–0.245

*: Ref.2; $\Delta = 100 \times$ [B3LYP – MP2] / B3LYP.

Table S4. The equilibrium rotational constants of *trans*-$CH_2(OH)_2$ predicted with B3LYP and other methods [1,2] using the same basis set aug-cc-pVTZ.

Method	Rotational constant (cm^{-1})		
	A	B	C
B3LYP	1.4001	0.3375	0.2996
B3LYP [a]	1.4000	0.3375	0.2995
MP2 [a]	1.3977	0.3401	0.3014
QCISD [a]	1.3973	0.3419	0.3028
CCSD(T) [a]	1.3899	0.3397	0.3008
MP2 [b]	1.3981	0.3399	0.3013

[a]: Ref. 1; [b]: Ref. 2. [b]These values were not specified to correspond to the rotational constants at equilibrium or vibrationally-ground state.

Table S5. Comparison of the difference of predicted absolute energies (ΔE) and Gibb's free energies (ΔG) of *trans*-$CH_2(OH)_2$ and *cis*-$CH_2(OH)_2$: ΔE or ΔG = *trans*-$CH_2(OH)_2$ – *cis*-$CH_2(OH)_2$. The basis set aug-cc-pVTZ was employed in this work and the previous report [1].

Method	ΔE in kcal mol^{-1}	ΔG (298 K) in kcal mol^{-1}
B3LYP	–2.20	–2.01
B3LYP*	–2.26	–1.65
MP2*	–2.38	–1.72
QCISD*	–2.35	–1.68

*: Ref. 1.

Table S6. Optimized molecular structures of *trans*- and *cis*-$CH_2(OH)_2$, $CD_2(OH)_2$, $CD_2(OH)_2$, and $CD_2(OD)_2$ determined with B3LYP/aug-cc-pVTZ. (bond length (*d*): angstrom; bond angle (∠): degree; dihedral angle (*ϕ*): degree).

parameter	*trans*-methanediol				*cis*-methanediol			
	$CH_2(OH)_2$	$CD_2(OH)_2$	$CH_2(OD)_2$	$CD_2(OD)_2$	$CH_2(OH)_2$	$CD_2(OH)_2$	$CH_2(OD)_2$	$CD_2(OD)_2$
$d(C–O_1)$	1.4082	1.4082	1.4082	1.4082	1.4092	1.4092	1.4092	1.4092
$d(C–O_2)$	1.4081	1.4081	1.4081	1.4081	1.4091	1.4091	1.4091	1.4091
$d(O_1–H_1)$	0.9635	0.9635	0.9635	0.9635	0.9620	0.9620	0.9620	0.9620
$d(O_2–H_2)$	0.9636	0.9636	0.9636	0.9636	0.9620	0.9620	0.9620	0.9620
$d(C–H_3)$	1.0914	1.0914	1.0914	1.0914	1.0954	1.0954	1.0954	1.0954
$d(C–H_4)$	1.0914	1.0914	1.0914	1.0914	1.0866	1.0866	1.0866	1.0866
$\angle O_1CO_2$	112.9942	112.9942	112.9942	112.9942	113.9044	113.9044	113.9044	113.9044
$\angle H_1O_1C$	108.5327	108.5327	108.5327	108.5327	109.9392	109.9392	109.9392	109.9392
$\angle H_2O_2C$	108.5351	108.5351	108.5351	108.5351	109.9427	109.9427	109.9427	109.9427
$\angle H_3CO_2$	105.1985	105.1985	105.1985	105.1985	110.4953	110.4953	110.4953	110.4953
$\angle H_3CO_1$	111.7888	111.7888	111.7888	111.7888	110.4816	110.4816	110.4816	110.4816
$\angle H_4CO_1$	105.2043	105.2043	105.2043	105.2043	105.8779	105.8779	105.8779	105.8779
$\angle H_4CO_2$	111.7861	111.7861	111.7861	111.7861	105.8708	105.8708	105.8708	105.8708
$\phi H_1O_1CO_2$	62.7796	62.7796	62.7796	62.7796	79.2727	79.2727	79.2727	79.2727
$\phi H_2O_2CO_1$	62.7907	62.7907	62.7907	62.7907	–79.0590	–79.0590	–79.0590	–79.0590
$\phi H_3CO_2O_1$	122.2166	122.2166	122.2166	122.2166	125.0489	125.0489	125.0489	125.0489
$\phi H_4CO_1O_2$	122.2171	122.2171	122.2171	122.2171	115.9168	115.9168	115.9168	115.9168

Table S7. The absolute energies and Gibb's free energy difference at 298 K (hartrees) of *trans*- and *cis*-$CH_2(OH)_2$, $CD_2(OH)_2$, $CH_2(OD)_2$, and $CD_2(OD)_2$ and ΔE or ΔG = *trans* – *cis* predicted using B3LYP/aug-cc-pVTZ including zero-point energy. The values of ΔE and ΔG in kcal mol^{-1} are presented in the parentheses.

Conformer	Molecules			
	$CH_2(OH)_2$	$CD_2(OH)_2$	$CH_2(OD)_2$	$CD_2(OD)_2$
trans	–190.9808	–190.9877	–190.9875	–190.9943
cis	–190.9773	–190.9841	–190.9838	–190.9907
ΔE	–0.0035 (–2.20)	–0.0036 (–2.26)	–0.0037 (–2.32)	–0.0036 (–2.26)
trans	–191.0058	–191.0129	–191.0129	–191.0200
cis	–191.0026	–191.0097	–191.0096	–191.0168
ΔG (298 K)	–0.0032 (–2.01)	–0.0032 (–2.01)	–0.0033 (–2.07)	–0.0032 (–2.01)

Table S8. Harmonic wavenumber (cm^{-1}) and the IR intensity (km mol^{-1}) of $CH_2(OH)_2$ predicted using B3LYP/aug-cc-pVTZ. Anharmonic wavenumber and corresponding infrared intensity are provided in the parentheses.

	Vibrational mode	*trans*-$CH_2(OH)_2$			Vibrational mode	*cis*-$CH_2(OH)_2$	
		B3LYP/aug-cc-pVTZ				B3LYP/aug-cc-pVTZ	
		Wavenumber	Intensity			Wavenumber	Intensity
ν_1	OH stret.	3795 (3617)	24 (27)	ν_1	OH stret.	3812 (3623)	19 (18)
ν_2	OH stret.	3794 (3612)	44 (28)	ν_2	OH stret.	3810 (3622)	39 (31)
ν_3	CH_2 stret.	3077 (2937)	38 (43)	ν_3	CH_2 stret.	3121 (2980)	21 (26)
ν_4	CH_2 stret.	3031 (2897)	55 (36)	ν_4	CH_2 stret.	2993 (2864)	71 (53)
ν_5	CH_2 sciss.	1526 (1486)	0 (0)	ν_5	CH_2 sciss.	1514 (1478)	0 (0)
ν_6	CH_2 wag	1442 (1413)	49 (55)	ν_6	CH_2 wag	1436 (1404)	23 (23)
ν_7	CH_2 twist	1388 (1354)	3 (3)	ν_7	CH_2 rock	1404 (1363)	20 (14)
ν_8	COH bend	1368 (1311)	34 (15)	ν_8	CH_2 twist	1369 (1320)	3 (1)
ν_9	COH bend + CH_2 wag	1202 (1176)	2 (2)	ν_9	COH bend + CH_2 wag	1162 (1149)	75 (45)
ν_{10}	OCO asym. stret.	1045 (1012)	285 (289)	ν_{10}	OCO sym. stret.	1053 (1029)	33 (23)
ν_{11}	OCO sym. stret.	1030 (1003)	92 (92)	ν_{11}	OCO asym. stret.	1035 (1004)	307 (304)
ν_{12}	CH_2 rock	1006 (997)	5 (3)	ν_{12}	CH_2 rock	993 (980)	50 (56)
ν_{13}	OCO bend	554 (532)	60 (45)	ν_{13}	OCO bend	534 (526)	24 (8)
ν_{14}	COH torsion	376 (362)	61 (80)	ν_{14}	COH torsion	381 (307)	117 (99)
ν_{15}	COH torsion	367 (316)	160 (135)	ν_{15}	COH torsion	178 (63)	71 (41)

Table S9. Harmonic wavenumber (cm^{-1}) and the IR intensity (km mol^{-1}) of $CD_2(OH)_2$ using predicted B3LYP/aug-cc-pVTZ. Anharmonic wavenumber and corresponding infrared intensity are provided in the parentheses.

	Vibrational mode	*trans*-$CD_2(OH)_2$			Vibrational mode	*cis*-$CD_2(OH)_2$	
		B3LYP/aug-cc-pVTZ				B3LYP/aug-cc-pVTZ	
		Wavenumber	Intensity			Wavenumber	Intensity
ν_1	OH stret.	3795 (3618)	24 (27)	ν_1	OH stret.	3812 (3624)	18 (17)
ν_2	OH stret.	3794 (3612)	45 (29)	ν_2	OH stret.	3810 (3622)	40 (31)
ν_3	CD_2 stret.	2295 (2214)	28 (29)	ν_3	CD_2 stret.	2317 (2219)	18 (16)
ν_4	CD_2 stret.	2199 (2082)	40 (23)	ν_4	CD_2 stret.	2182 (2071)	49 (25)
ν_5	COH bend	1329 (1283)	98 (77)	ν_5	COH bend + CD_2 rock	1355 (1315)	24 (21)
ν_6	COH bend + CD_2 scis.	1304 (1270)	8 (6)	ν_6	COH bend + CD_2 twist	1243 (1201)	80 (58)
ν_7	CD_2 sciss.	1134 (1110)	25 (23)	ν_7	CD_2 sciss.	1137 (1118)	19 (14)
ν_8	CD_2 wag	1118 (1088)	144 (128)	ν_8	CD_2 wag	1112 (1084)	157 (135)
ν_9	OCO sym. stret.	994 (973)	54 (59)	ν_9	OCO sym. stret.	992 (973)	40 (41)
ν_{10}	OCO asym. stret.	982 (963)	113 (127)	ν_{10}	OCO asym. stret.	984 (962)	148 (159)
ν_{11}	CD_2 twist	915 (895)	5 (2)	ν_{11}	CD_2 twist	925 (903)	24 (21)
ν_{12}	CD_2 rock	846 (834)	22 (20)	ν_{12}	CD_2 rock	842 (833)	14 (15)
ν_{13}	OCO bend	548 (526)	62 (47)	ν_{13}	OCO bend	526 (519)	25 (8)
ν_{14}	COH torsion	374 (362)	59 (77)	ν_{14}	COH torsion	376 (303)	123 (94)
ν_{15}	COH torsion	362 (312)	154 (132)	ν_{15}	COH torsion	178 (65)	70 (42)

Table S10. Harmonic wavenumber (cm^{-1}) and the IR intensity (km mol^{-1}) of $CH_2(OD)_2$ predicted using B3LYP/aug-cc-pVTZ. Anharmonic wavenumber and corresponding infrared intensity are provided in the parentheses.

	Vibrational mode	*trans*-$CH_2(OD)_2$			Vibrational mode	*cis*-$CH_2(OD)_2$	
		B3LYP/aug-cc-pVTZ				B3LYP/aug-cc-pVTZ	
		Wavenumber	Intensity			Wavenumber	Intensity
ν_1	CH_2 stret.	3078 (2936)	34 (40)	ν_1	CH_2 stret.	3122 (2983)	17 (22)
ν_2	CH_2 stret.	3032 (2899)	52 (35)	ν_2	CH_2 stret.	2993 (2867)	71 (52)
ν_3	OD stret.	2762 (2664)	19 (19)	ν_3	OD stret.	2775 (2675)	14 (13)
ν_4	OD stret.	2761 (2669)	31 (19)	ν_4	OD stret.	2773 (2674)	28 (21)
ν_5	CH_2 sciss.	1526 (1488)	0 (0)	ν_5	CH_2 sciss.	1514 (1477)	0 (0)
ν_6	CH_2 wag	1430 (1398)	20 (17)	ν_6	CH_2 wag	1432 (1403)	16 (14)
ν_7	CH_2 twist	1326 (1291)	0 (0)	ν_7	CH_2 twist	1334 (1298)	0 (0)
ν_8	COD bend + CH_2 rock	1235 (1208)	15 (14)	ν_8	COD bend + CH_2 rock	1244 (1213)	7 (7)
ν_9	OCO sym. stret.	1069 (1040)	43 (38)	ν_9	OCO sym. stret.	1043 (1026)	58 (47)
ν_{10}	OCO asym. stret.	1042 (1008)	270 (262)	ν_{10}	OCO asym. stret.	1034 (1006)	293 (258)
ν_{11}	COD bend + CH_2 twist	919 (900)	32 (33)	ν_{11}	COD bend + CH_2 twist	878 (861)	48 (52)
ν_{12}	COD bend + CH_2 rock	833 (826)	23 (22)	ν_{12}	COD bend + CH_2 rock	849 (836)	18 (17)
ν_{13}	OCO bend	519 (505)	38 (32)	ν_{13}	OCO bend	523 (509)	24 (16)
ν_{14}	COD torsion	283 (240)	95 (70)	ν_{14}	COD torsion	284 (241)	54 (49)
ν_{15}	COD torsion	273 (269)	37 (57)	ν_{15}	COD torsion	131 (44)	39 (22)

Table S11. Harmonic wavenumber (cm^{-1}) and the IR intensity (km mol^{-1}) of $CD_2(OD)_2$ predicted using B3LYP/aug-cc-pVTZ. Anharmonic wavenumber and corresponding infrared intensity are provided in the parentheses.

	Vibrational mode	*trans*-$CD_2(OD)_2$			Vibrational mode	*cis*-$CD_2(OD)_2$	
		B3LYP/aug-cc-pVTZ				B3LYP/aug-cc-pVTZ	
		Wavenumber	Intensity			Wavenumber	Intensity
ν_1	OD stret.	2762 (2670)	16 (19)	ν_1	OD stret.	2775 (2676)	14 (14)
ν_2	OD stret.	2762 (2664)	28 (19)	ν_2	OD stret.	2774 (2674)	25 (20)
ν_3	CD_2 stret.	2294 (2184)	27 (11)	ν_3	CD_2 stret.	2316 (2244)	19 (14)
ν_4	CD_2 stret.	2199 (2079)	42 (25)	ν_4	CD_2 stret.	2182 (2073)	49 (29)
ν_5	CD_2 sciss.	1161 (1140)	12 (10)	ν_5	CD_2 sciss.	1152 (1130)	5 (5)
ν_6	CD_2 wag	1132 (1102)	177 (140)	ν_6	COD bend + CD_2 sciss.	1116 (1088)	21 (19)
ν_7	COD bend + CD_2 wag	1097 (1072)	18 (19)	ν_7	CD_2 wag	1112 (1085)	168 (125)
ν_8	COD bend + CD_2 twist	1033 (1014)	0 (0)	ν_8	CD_2 twist	1009 (982)	14 (45)
ν_9	OCO sym. stret.	988 (965)	46 (46)	ν_9	OCO sym. stret.	989 (970)	40 (39)
ν_{10}	OCO asym. stret.	980 (958)	112 (125)	ν_{10}	OCO asym. stret.	981 (959)	135 (114)
ν_{11}	CD_2 twist	858 (844)	10 (11)	ν_{11}	COD bend + CD_2 twist	834 (819)	41 (42)
ν_{12}	CD_2 rock	744 (717)	24 (15)	ν_{12}	COD bend + CD_2 rock	754 (755)	9 (6)
ν_{13}	OCO bend	514 (500)	39 (33)	ν_{13}	OCO bend	514 (501)	25 (17)
ν_{14}	COD torsion	277 (235)	90 (70)	ν_{14}	COD torsion	278 (236)	58 (48)
ν_{15}	COD torsion	272 (269)	37 (53)	ν_{15}	COD torsion	131 (46)	39 (23)

Table S12. Rotational parameters of *trans*-$CH_2(OH)_2$ at ground state v″ = 0 and first vibrationally-excited state v' = 1 for different vibrational modes.

Vibrational mode	*trans*-$CH_2(OH)_2$							
		Rotational constant (cm^{-1})						Transition type
		A	B	C	A' / A″	B' / B″	C' / C″	
	$v''=0$	1.3859	0.3350	0.2966				
OCO asym. stret.	$v'_{10}=1$	1.3761	0.3337	0.2945	0.9929	0.9961	0.9929	*a*-type
OCO sym. stret.	$v'_{11}=1$	1.3921	0.3335	0.2959	1.0045	0.9955	0.9976	*b*-type

Table S13. Rotational parameters of *trans*-$CD_2(OH)_2$ at ground state v″ = 0 and first vibrationally-excited state v' = 1 for different vibrational modes.

Vibrational mode	*trans*-$CD_2(OH)_2$							
″		Rotational constant (cm^{-1})						Transition type
		A	B	C	A' / A″	B' / B″	C' / C″	
	$v''=0$	1.0244	0.3245	0.2832				
COH bending	$v'_5=1$	1.0265	0.3246	0.2832	1.0020	1.0003	1.0000	*a*-type : *c*-type = 0.9 : 0.1
CD_2 wagging	$v'_8=1$	1.0227	0.3231	0.2818	0.9983	0.9957	0.9951	*a*-type
OCO sym. stret.	$v'_9=1$	1.0256	0.3235	0.2823	1.0012	0.9969	0.9968	*b*-type
OCO asym. stret.	$v'_{10}=1$	1.0194	0.3241	0.2826	0.9951	0.9988	0.9979	*a*-type

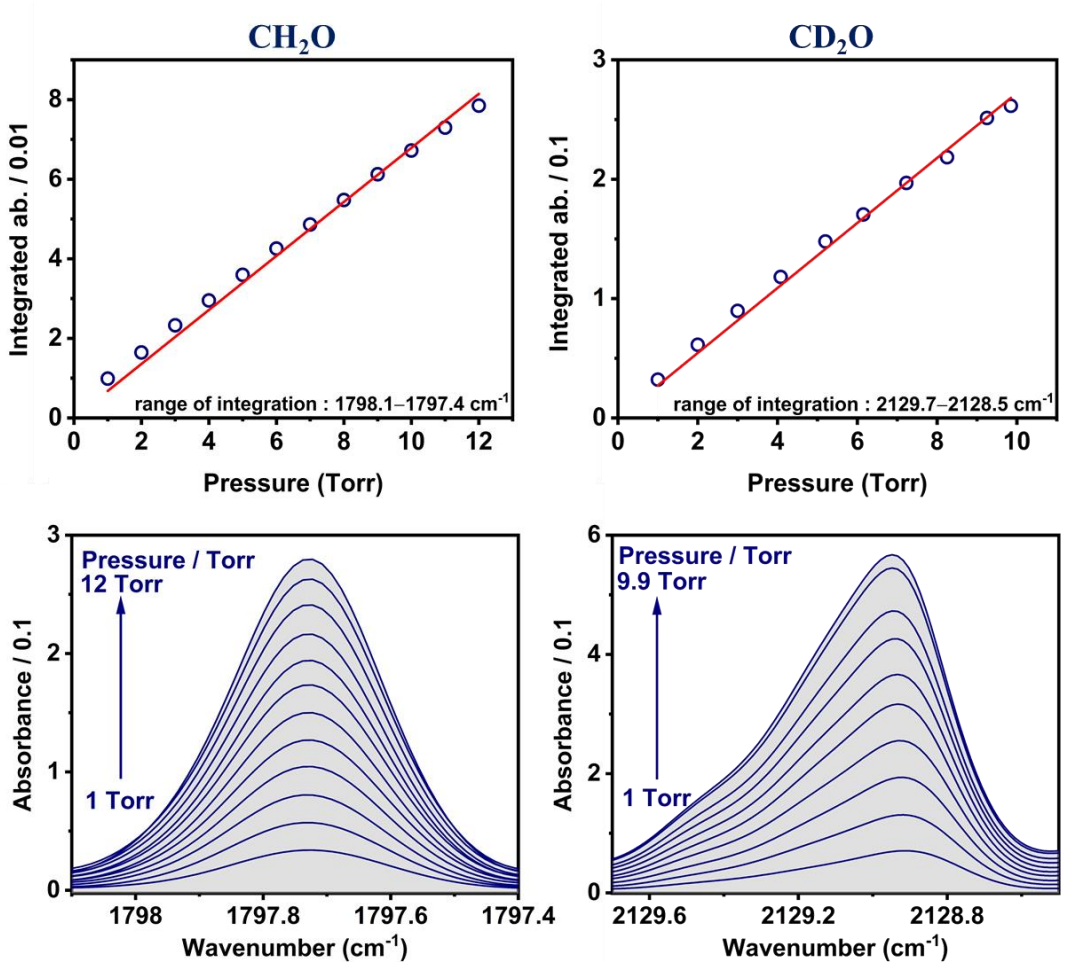
CH2O
CD2O
Integrated ab. / 0.01
Integrated ab. / 0.1
range of integration : 1798.1–1797.4 cm-1
range of integration : 2129.7–2128.5 cm-1
Pressure (Torr)
Pressure (Torr)
Pressure / Torr
12 Torr
1 Torr
Pressure / Torr
9.9 Torr
1 Torr
Absorbance / 0.1
Absorbance / 0.1
Wavenumber (cm-1)
Wavenumber (cm-1)

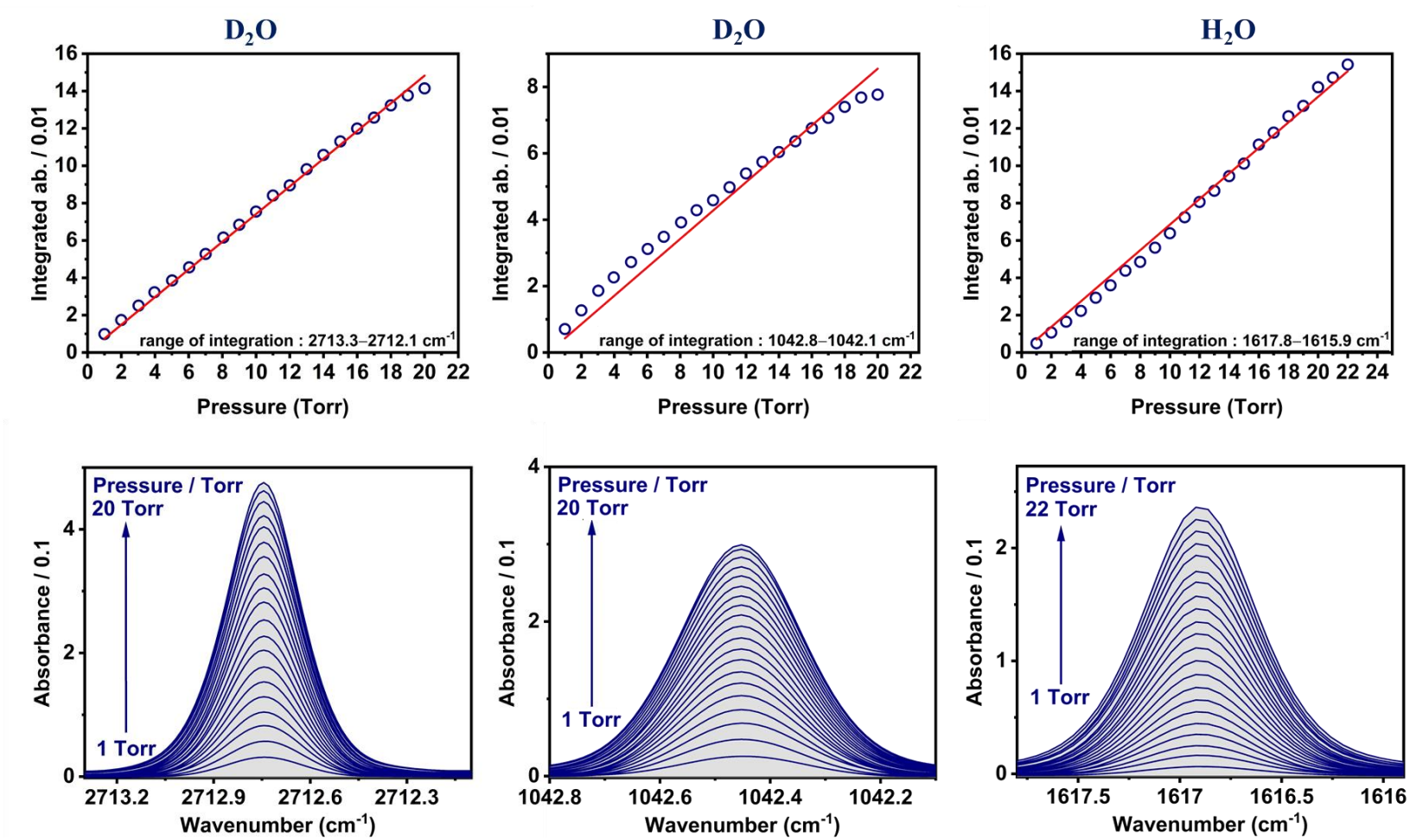

Figure S1. The pressures of the pure substances versus the integrated absorbances at given wavenumbers for deriving the partial pressures in the mixed samples.

trans-$CH_2(OH)_2$	*trans*-$CD_2(OH)_2$
(ν_{10}) OCO asym. stret.	(ν_5) COH bend
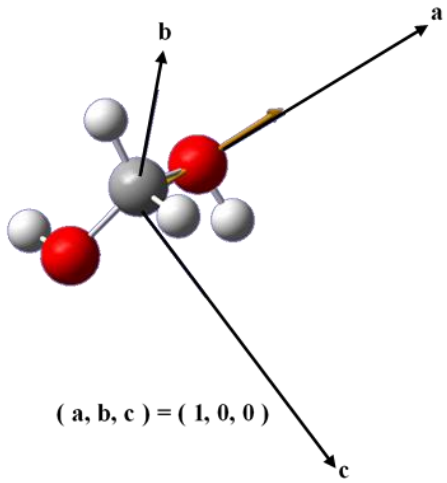	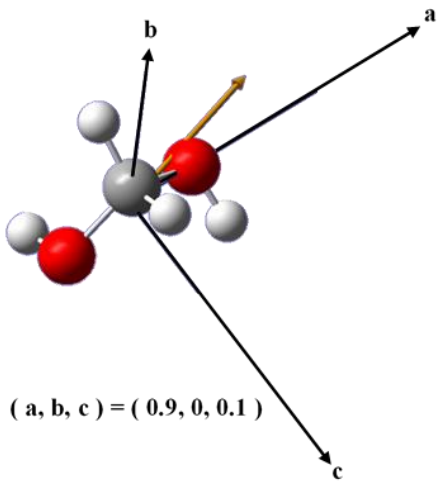
(ν_{11}) OCO sym. stret.	(ν_8) CD_2 wag
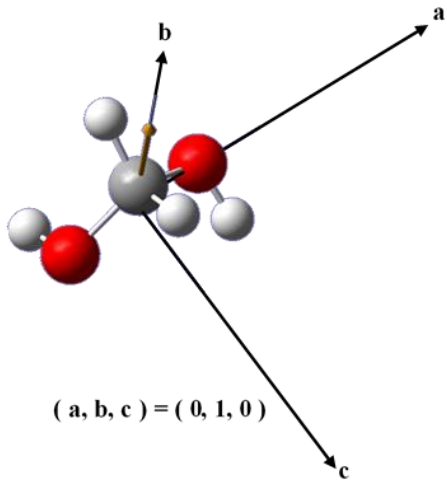	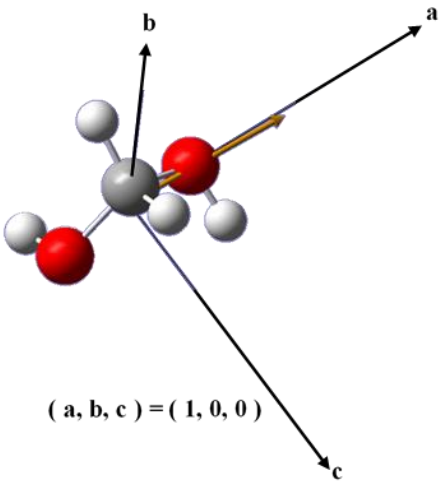

Figure S2. Dipole derivatives of relevant vibrations of *trans*-$CH_2(OH)_2$ and *trans*-$CD_2(OH)_2$.

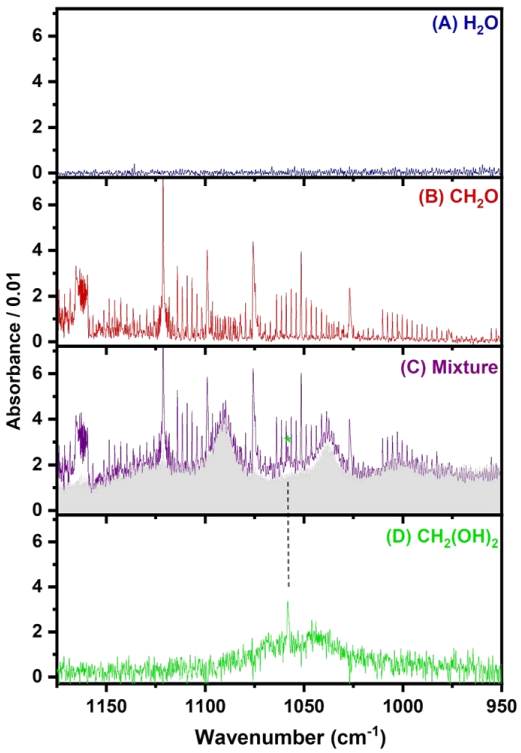

Figure S3. Gaseous IR absorption spectra of (A) H_2O, (B) CH_2O, and (C) mixture of (A) and (B) in the bath of N_2. The gray shadow denotes the IR spectrum of the deposit component on the BaF_2 window. (D) Difference spectrum by subtracting (C) with (A), (B), and the deposited component and multiplied by 2.5 to fit the scales in (A) and (B).

REFERENCES

[1] C. Barrientos, P. Redondo, H. Martínez and A. Largo, *Astrophys. J.*, 2014, **784**, 132.

[2] B. M. Hays and S. L. W. Weaver, *J. Phys. Chem. A*, 2013, **117**, 7142−7148.